CIRP Annals - Manufacturing Technology 00 (2025) 1–5

Contents lists available at ScienceDirect

CIRP Annals - Manufacturing Technology

journal homepage: https://www.editorialmanager.com/CIRP/default.aspx

Large-scale functional patterning using mobile robot swarms and ergodic control

Malachi Landis, Muye Jia, Annalisa T. Taylor, Todd D. Murphey, Ping Guo (2)*

Department of Mechanical Engineering, Northwestern University, Evanston, IL 60208, USA

ARTICLE INFO

Article history:
Available online xxx

Keywords:
Surface modification
Robot
Ergodic control

ABSTRACT

Large-scale surfaces, such as ship hulls, face challenges in applying functional structures due to manufacturing constraints. This work presents a scalable approach using low-cost, autonomous robot swarms guided by an ergodic control framework to pattern micro-scale features on meter-scale metallic surfaces. The robots operate collaboratively to achieve density-specific coverage, optimizing surface functionalities like friction reduction and hydrodynamic performance. Experimental validation demonstrates the critical role of feature density in tribological performance, and an example application highlights the creation of gradient-density patterns. This innovative method unlocks new possibilities for functional surface patterning on large-scale structures with imprecise robots.

© 2025 CIRP. Published by Elsevier Ltd. All rights are reserved, including those for text and data mining, AI training, and similar technologies.

1. Introduction

Engineering surfaces can be enhanced by incorporating arrays of structural features, such as dimples and grooves, which unlock various functionalities that go beyond the material's bulk properties. These features, ranging in size from millimeters to nanometers, provide benefits like reducing icing [1], resisting biological material accumulation [2], generating hydrodynamic lift [3], capturing wear particles [4], altering wetting behavior [5], and reducing drag from skin friction [6]. One particularly impactful application is friction reduction, which has the potential to lower greenhouse gas emissions and waste, as friction accounts for 20% of global energy consumption [7]. However, applying functional structures to large-scale surfaces like cargo vessel hulls presents significant challenges. Traditional manufacturing methods—such as lithography, precision machining, laser surface texturing, micro-casting, and etching—are often sophisticated but do not scale efficiently for large workpieces [8,9,10]. While effective for smaller components, these techniques become impractical for large structures, necessitating innovative and scalable approaches to pattern the surface on a larger scale.

For small components, techniques like laser surface texturing are well-suited to the manufacturing process and align with the traditional approach where the *workpiece is much smaller than the tool*. As the workpiece becomes larger, such as in airplanes or cargo ships, these techniques become infeasible to apply directly. Sometimes, for example with drag-reducing riblets, films containing functional structures may be precisely manufactured elsewhere and applied separately to the workpiece [6]. Functional random patterns may be applied in situ by spraying but may require significant human labor [11]. Robots may alleviate this combined manufacturing and labor constraint, as has already been demonstrated for use in ship cleaning [12,13]. However, complex, single-robot systems are often expensive and may not scale effectively. Research on mobile robot swarms for manufacturing is limited and primarily focuses on explicit task division and coordinated collaboration [14,15].

We address this manufacturing challenge, patterning micro-scale features on a large-scale surface, by proposing multi-robot swarms that work collaboratively without explicit task division or communication. There are two key novelties in our approach. First, we design scalable, low-cost mobile robots with reciprocating patterning motion that can conquer large-scale surfaces. Second, we implement *ergodic control*, a unique framework which guides agents to effectively cover a surface collaboratively following a given coverage distribution target. Over the long run, each robot will spend time in locations proportional to the specified spatial distribution, e.g., the desired density of micro-features. This framework is ideal for planning low-cost mobile robots that do not have the precision required to place micro-features at exact locations and cannot be orchestrated by the simple raster scanning strategies of conventional machine tools. Ergodic control is effective for our large-scale functional patterning task because, for micro-structured functional surfaces, pattern density is more important than exact placement for surface functionality [16,17].

Our idea is illustrated in Fig. 1(a), where multiple robots collaboratively pattern a steel substrate according to an image of the Arc de Triomphe de l'Étoile [18]. Dark regions correlate to a high density of micro-scale dimples. Robots independently make control decisions while using global position feedback to achieve desired area coverages. The overarching vision is to scale the system (perhaps to thousands as in [19]) to allow robots to collectively work on extremely large surfaces, such as a ship hull as shown in Fig. 1(b), to improve fuel economy.

In Section 2, we detail the mobile robot design, shown later in teams of 3 and 5. Section 3 gives the implementation of ergodic control. In Section 4, we test our assumption of the importance of surface feature density on functional performance by varying the surface feature (dimple) density while measuring friction. Based on the findings, in Section 5, we

* Corresponding author.
E-mail address: ping.guo@northwestern.edu (P. Guo).

https://doi.org/10.1016/j.cirp.2025.04.044

0007-8506/© 2025 CIRP. Published by Elsevier Ltd. All rights are reserved, including those for text and data mining, AI training, and similar technologies.

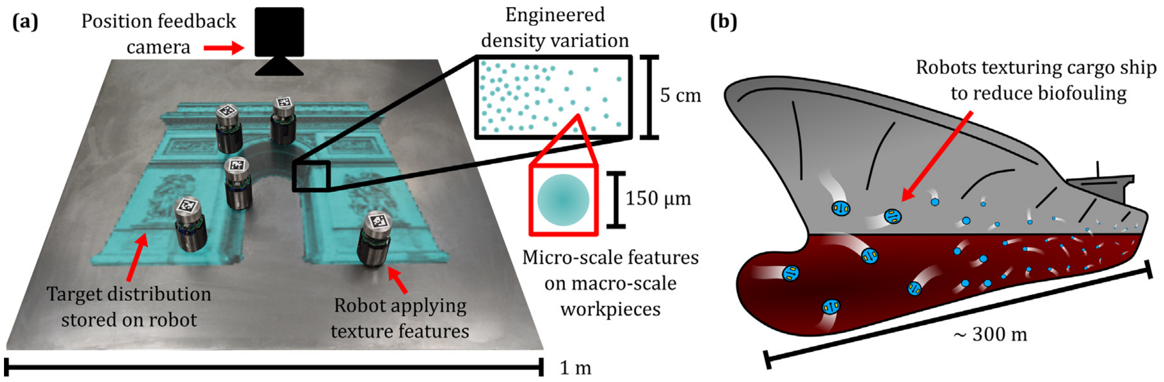
(a)
Position feedback camera
Engineered density variation
5 cm
150 μm
Micro-scale features on macro-scale workpieces
Target distribution stored on robot
Robot applying texture features
1 m
(b)
Robots texturing cargo ship to reduce biofouling
~ 300 m

Fig. 1. (a) Five robots collaborate to pattern a steel substrate with an image of the Arc de Triomphe de l'Étoile [14], which has been digitally overlaid on the surface to illustrate their collective objective. (b) A cartoon illustration of robots collectively patterning a cargo ship to improve fuel economy.

demonstrate our swarm patterning workflow to create a patterned surface with gradient densities of dimples for optimal friction reduction. In summary, this work demonstrates a complete swarm patterning workflow from robot design and ergodic control to the demonstration of micro-dimple patterning on a meter-scale workpiece.

2. Mobile robot patterning system

Our robots are designed to be low-cost (<$100) and compact (75 mm diameter), with onboard intelligence to run control algorithms, as shown in Fig. 2(a). This enables scalability for deployment as a robot swarm. A reciprocating indentation mechanism is designed to pattern dimple features approximately 180 μm in diameter using a 60° carbide tip at up to 4 Hz. These robots can function either independently or collectively, traversing meter-scale metallic substrates at up to 75 mm/s while creating micro-scale features.

Several design considerations were made to lower cost, decrease size, and improve performance. A flexure-based mechanism is proposed to achieve the reciprocating motion of the patterning tool, shown schematically in Fig. 2(b) and in CAD in Fig. 2(c). The rotation of a cam forces the tool upwards, and a pair of blade flexures arranged at a 60° angle constrain the motion in a linear path while accumulating elastic energy to drive the indentation tool into the workpiece. After one cam revolution, the indentation tool drops downward and impacts the surface, leaving a dimple. The tip of the indentation tool is carbide while the body is steel for additional impact. A button mounted on the underside of the PCB is depressed by the indentation tool at the top of its stroke, allowing the tool to be left retracted if indentation is not desired. Most structural components were 3D printed from ABS plastic on a desktop printer (Bambulab X1C), including the body, wheels, flexure assembly, and AprilTag/mass mount. The steel and carbide indentation tool, along with an added steel mass for traction, were the only machined components and were simple to fabricate on manual equipment. The detailed robot design is released in our open repository [20].

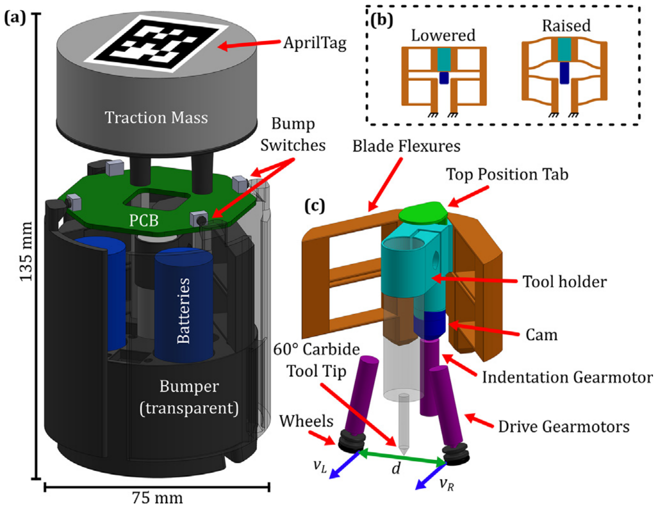

Fig. 2. (a) Robot CAD model. (b) Schematic of indentation mechanism motion. (c) View of indentation mechanism and wheels with velocities v_L and v_R separated by a distance $d = 29.6$ mm.

A custom Printed Circuit Board (PCB) contains the robot's electronics. A 240 MHz, dual-core microcontroller with 325 kB of dynamic memory (SeeedStudio XIAO ESP32S3 Sense) runs control algorithms onboard and communicates externally using Bluetooth

Low Energy (BLE) 5.0. Four buttons are mounted on the periphery of the board and are depressed by printed paddles mounted to the robot base. These bump sensors detect impacts against another robot or the environment and allow for collisions to be resolved automatically. The robot is powered by two, 2.2 A-hour, 18,650 lithium-ion batteries (Adafruit 1781) which have been shown to provide at least 2 h of runtime. Three 200 RPM gear motors (INEED MOTOR IND-GM-615–136) are used: two for the main drive wheels and one for the indentation mechanism. The drive motors are mounted at a 12° angle from vertical to minimize the robot footprint and move the wheel contact patches toward the center of the robot to maximize turning speed.

The robot communicates with a central computer through BLE using Python (via `Bleak` [21]). This central computer processes overhead images using `OpenCV` and measures robot positions using `AprilTag` [22] while simultaneously storing data from the patterning process. Robots receive position feedback over BLE to update their controls. The size of the workpiece is *constrained only by the position feedback method*, as illustrated in Fig. 1(a). The robots are demonstrated operating in teams of 3 and 5, collectively applying patterns to a workpiece covering an area of 1.0 m^2.

3. Ergodic control for patterning

Controlling these robots to pattern large-scale workpieces is nontrivial. An effective algorithm must allow multiple robots to collaborate easily and robustly while achieving surface functionality. Traditional raster scanning (e.g., precise back-and-forth motion along predefined linear paths) and careful division of the domain between robots dominates conventional coverage path planning [23] but is insufficient for the relatively low accuracy and collaborative nature of our robots. We therefore leverage a key assumption: density is more important than exact placement for surface functionality. This assumption enables ergodic control, which relies on two ideas: (1) a goal (e.g., image, pattern distribution) can be adequately represented as a probability distribution; (2) this distribution has a representation amenable to optimal control, in our case Fourier space.

Taken together, ergodic control seeks to drive an agent to effectively sample a target distribution by making comparisons between the agent's current coverage trajectory and the target distribution within Fourier space. Critically, this comparison has readily available derivatives, a key ingredient for optimal control. Ergodic control ensures that the robots will spend time in locations proportional to the specified spatial distribution. The term "ergodic" originates from ergodic theory in mathematics, which deals with systems that, over time, cover all regions of their state space in proportion to their statistical importance.

For the following, we consider a two-dimensional, unit domain. Controls are computed in this domain for simplicity and consistent control weights across real domain sizes. For a complete derivation of the coverage objective, see [24,25]. Following [24], we use cosine basis functions $F_{\mathbf{k}}(\mathbf{x})$ where $\mathbf{x} = (x, y)$ is the robot position (measured from the camera). A bold $\mathbf{k}$ indicates a $K \times K$ matrix in Fourier space, where K is the number of basis functions in each dimension. Higher values of K more accurately represent a distribution but require more computation and memory.

$$F_{\mathbf{k}}(\mathbf{x}) = \frac{1}{h_{\mathbf{k}}} \cos(k_x \pi x) \cos(k_y \pi y) \tag{1}$$

The $h_{\mathbf{k}}$ normalizing term is described in [24]. We represent the $N \times N$ pixel target distribution ϕ in Fourier space, $\phi_{\mathbf{k}}$, as:

$$\phi_{\mathbf{k}} = \frac{1}{N^2} \sum_{i=0}^{N-1} \sum_{j=0}^{N-1} \phi\left(\frac{i+1/2}{N}, \frac{j+1/2}{N}\right) F_{\mathbf{k}}\left(\frac{i+1/2}{N}, \frac{j+1/2}{N}\right) \tag{2}$$

The Fourier representation $c_{\mathbf{k}}$ of the robot trajectory could be calculated from a time series of points or can be incrementally updated at each time T with time step Δt, beginning from a zero matrix, saving memory and computational effort.

$$c_{\mathbf{k}}(t = T + \Delta t, \mathbf{x}) = \frac{T c_{\mathbf{k}}(t = T) + \Delta t F_{\mathbf{k}}(\mathbf{x})}{T + \Delta t} \tag{3}$$

We can now provide an ergodic metric $\mathcal{E}$ that compares the Fourier representation of the coverage objective, $\phi_{\mathbf{k}}$, and agent trajectory, $c_{\mathbf{k}}$. The coefficient $\Lambda_{\mathbf{k}}$ weighs low-frequency terms more heavily than high-frequency terms [24]. Lower $\mathcal{E}$ is better.

$$\mathcal{E} = \sum_{\mathbf{k}=0}^{K-1} \Lambda_{\mathbf{k}} (c_{\mathbf{k}} - \phi_{\mathbf{k}})^2 \tag{4}$$

The derivative of $\mathcal{E}$ requires the derivative of the trajectory representation $c_{\mathbf{k}}$ given in Eq. (6). In practice, neglecting $\Delta t/(T + \Delta t)$ allows agents to make consistent progress over long times.

$$\frac{\partial c_{\mathbf{k}}}{\partial \mathbf{x}} = \left(\frac{\Delta t}{T + \Delta t}\right) \frac{-1}{h_{\mathbf{k}}} \begin{bmatrix} k_x \pi \sin(k_x \pi x) \cos(k_y \pi y) \\ k_y \pi \cos(k_x \pi x) \sin(k_y \pi y) \end{bmatrix} \tag{6}$$

If features are being pre-planned directly, the above equations are sufficient for typical optimization schemes. For online control, we use Model Predictive Control (MPC), which is a receding horizon control scheme which requires modeling the robot dynamics f [26]. The robot has state $\mathbf{x}$, composed of positions x, y and angle θ, and controls $\mathbf{u}$, composed of wheel velocities v_L and v_R with separation d. The derivatives of these dynamics with respect to the state and controls are straightforward.

$$\mathbf{x} = \begin{bmatrix} x \\ y \\ \theta \end{bmatrix} \quad \mathbf{u} = \begin{bmatrix} v_L \\ v_R \end{bmatrix} \quad f = \begin{bmatrix} \dot{x} \\ \dot{y} \\ \dot{\theta} \end{bmatrix} = \begin{bmatrix} cos(\theta)(v_L + v_R)/2 \\ sin(\theta)(v_L + v_R)/2 \\ (-v_L + v_R)/d \end{bmatrix} \tag{7}$$

Within the MPC objective l, we add barrier function $\mathcal{B}$ which tends to keep the robot within a desired region. Values of $\mathcal{B}$ are found by repeatedly detecting and expanding the edges on a binarized version of the target distribution. Gradients are then calculated numerically which automatically point toward the nearest edge. Practically, this gradient is stored onboard as an $N \times N$ lookup table. The gradient in each direction is an integer in the range $[-2, 2]$, so the two directions are encoded together within a single char to reduce memory consumption.

We use the shooting method to simulate the robot forward in time over n steps, incrementing $\mathbf{x}$ using f, beginning from $\mathbf{x}_0$. We proceed backward in time to generate the adjoint variable $\boldsymbol{\rho}$ for each step using $\dot{\boldsymbol{\rho}}$, beginning with $\boldsymbol{\rho}_{n-1} = 0$, then decrement each control in the horizon using $\Delta \mathbf{u}$.

$$l = \mathcal{E} + \mathcal{B} \qquad \dot{\boldsymbol{\rho}} = -\left(\frac{\partial f}{\partial \mathbf{x}}\right)^T \boldsymbol{\rho} - \frac{\partial l}{\partial \mathbf{x}} \qquad \Delta \mathbf{u} = \left(\frac{\partial f}{\partial \mathbf{u}}\right)^T \boldsymbol{\rho} \tag{8}$$

These expressions have been implemented in both C++ for onboard the robot and Python/JAX for simulation and control parameter tuning. See our GitHub repository for details [20].

Algorithm performance was measured on the microcontroller and shows time scaling nearly linearly with MPC horizon steps n and nearly quadratically with the number of basis functions K in Table 1. Green values meet our 20 Hz update rate target, orange values do not, and blue values exhaust available memory.

Table 1
Control loop execution speed in ms for different K and n.

K \ n	5	10	15	20
10	2.5	5	7.5	10
20	7.5	14.5	21.5	28.5
30	15.5	29.5	44	58.5
40	26.5	51	75.5	100
50	40	78	115.5	OOM

It is important to clarify that *the robots collaborate without any direct communication with other robots*; rather, they collaborate through a shared task. Collisions between robots are detected by one of the bump sensors in each corner of the robot, then resolved by rotating to a random heading in the range [90, 270] degrees from that quadrant. This randomness allows robots to escape clusters without direct coordination while maintaining ergodicity through the molecular chaos assumption [27]. Fig. 3 shows a simulation result of 1 robot patterning alone for 5 h ($\mathcal{E} = 2 \times 10^{-3}$) compared to experimental position data for 5 robots patterning collaboratively for 1 h ($\mathcal{E} = 4 \times 10^{-5}$), both at the same patterning rate. See Movie S1 for footage of robot operation. The ergodic metric $\mathcal{E}$ measures coverage performance by comparing spatial frequencies of robot trajectories and the target pattern, so a low metric indicates a good match between robot motion and the desired texture distribution. Multiple robots, each running separate controllers, are better able to distribute their features than a single robot despite being identically programmed.

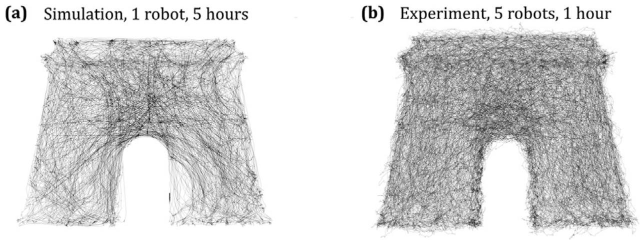

Fig. 3. (a) Simulated and (b) experimental trajectories from the ergodic control for the Arc de Triomphe in Fig. 1, with supplementary Movie S1.

4. Feature density effect on tribological performance

Our ergodic control scheme relies on the assertion that the density of features composing the functional surface is more important to the effectiveness of the surface than the exact relative positions of the features. In friction reduction applications, we show that high pattern densities are suitable for low-velocity sliding, while low pattern densities improve high-velocity sliding.

We experimentally verified the importance of density for the patterned features generated by our robots using a rotary tribometer (RTEC MFT-5000) pictured in Fig. 4(a) and shown schematically in Fig. 4(b). We mounted a robot indentation tool in a CNC motion stage and patterned features at multiple densities onto Al6061 cylinders (Fig. 4(c)). A representative dimple is shown in Fig. 4(d). No significant tool wear or change in dimple profile was observed over the production of approximately 50,000 total dimples. The surfaces were sanded to a roughness of 0.314 μm Ra, removing burrs around the dimples. The rear of each cylinder was conical to accept a pin which would apply a 150 N load while allowing the patterned face to tilt until flat against an Al6061 disk. Samples were submerged in 80W-90 gear oil (Lucas Oil). The disk was machined to a roughness of 0.211 μm Ra before each test. Multiple sliding velocities were tested for each density, with each velocity active for 5 min. The last 100 s of each velocity period were used for statistical analysis. Dimple coverage densities were fabricated at 0 (smooth surface), 2, 4, 8, 16 and 32%. Sliding velocities ranged from 0.05 to 1.6 m/s. Roughness was measured with a Zygo NewView 7300, and the dimple profile was measured with a Keyence VHX-7000.

Fig. 5 shows the average fiction coefficient at a given sliding velocity for each coverage density. Friction generally increased with increasing sliding velocity, as expected for hydrodynamic lubrication. Dimples generally reduced the coefficient of friction, agreeing with existing

Please cite this article as: M. Landis et al., Large-scale functional patterning using mobile robot swarms and ergodic control, CIRP Annals - Manufacturing Technology (2025), https://doi.org/10.1016/j.cirp.2025.04.044

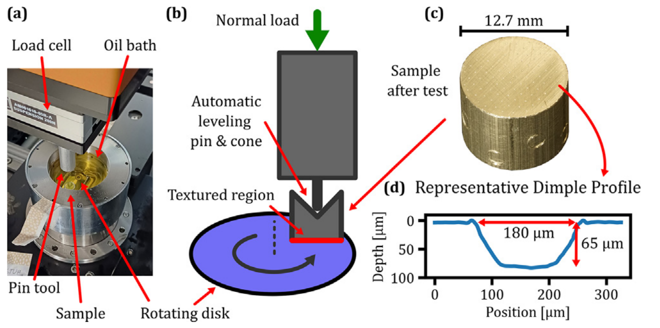

Fig. 4. (a) Setup and (b) schematic of rotary tribometer. (c) A patterned sample with 2% area coverage. (d) A single dimple profile in Al6061 alloy.

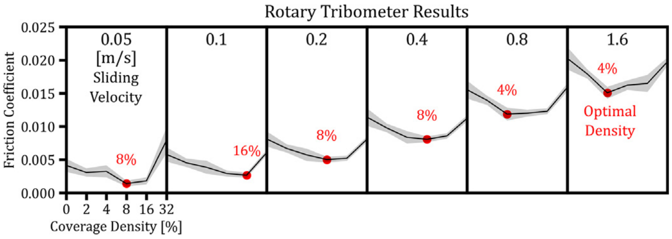

Fig. 5. Mean friction coefficients (black line) and 2σ error bars (grey regions) for each coverage density and sliding velocity, with the optimal (lowest friction) coverage highlighted.

literature which suggests surface features increase the pressure in the interface, thereby increasing separation of the sliding faces and lowering shear stress within the lubricant [9,10]. Coverage density strongly affects the coefficient of friction, and each sliding velocity was observed to have a certain density which yielded minimum friction. At lower sliding velocities, a pattern density between 8% to 16% yields the best friction reduction, while at higher sliding velocities, the optimal dimple density shifts towards 4%. The highest coverage density of 32% tended to increase friction, a similar trend to literature [10]. This phenomenon may be due to decreasing contact area and therefore increasing contact stress at the interface. A quadratic fit between sliding speed and optimal coverage was generated and applied in Section 5 for an optimal pattern design with varying densities.

5. Example of density-gradient patterning

To demonstrate the capabilities of our robot swarm and ergodic control in a practical scenario, we generated a micro-patterned surface designed for optimal tribological performance, targeting a gradient density distribution of dimples based on friction test results. As illustrated in Fig. 6(a), a hypothetical arm rotates sinusoidally through a 90-degree angle, with a load supported by a slider on a patterned plate. The slider experiences varying velocities depending on the arm's angular position, making a gradient pattern density on the plate natural, as shown in Fig. 6(b). Using the slider's velocity and the previously determined optimal density fit, a target pattern distribution was created (Fig. 6(c)) with high density near the outer edges (where the slider decelerates) and low density in the middle (where the slider moves fastest). Simulated robot trajectories (Fig. 6(d)) confirmed effective control parameters, validated by the decreasing ergodic metric $\mathcal{E}$ (defined in Eq. (4)) shown in Fig. 6(e).

The target was uploaded to a team of 3 robots which ran on a sheet of cold-rolled mild steel (σ_{ys}=172–241 MPa and σ_{UTS}= 262–345 MPa). See Movie S1. After 2 h, the robots were stopped and the resulting surface was imaged using low-angle illumination to highlight the dimples, shown in Fig. 7(a). Images of different pattern regions confirm the robots produced varying densities of dimples as per the target specification.

6. Conclusion

We present a low-cost robot swarm for surface patterning of micro-features and a control framework capable of scaling functional surface manufacturing beyond the size limitations of traditional techniques.

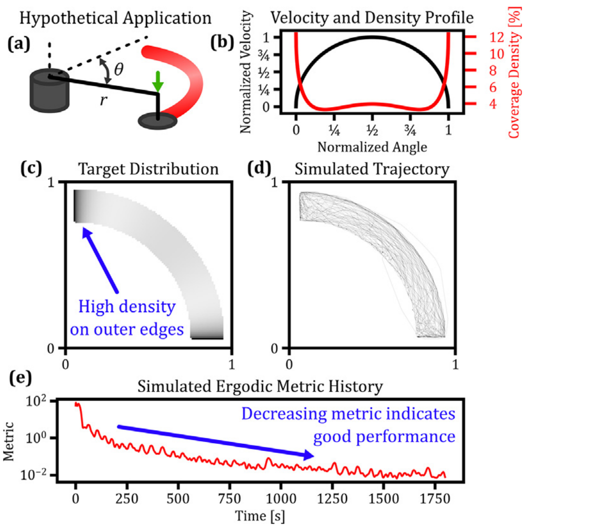

Fig. 6. (a) Schematic of rotating arm with slider. (b) Velocity and optimal density change with slider position. (c) Target distribution has low density where the slider moves quickly and high density near stops. (d) Simulation confirms acceptable robot behavior. (e) Persistent decrease in the ergodic metric indicates good approximation of the target.

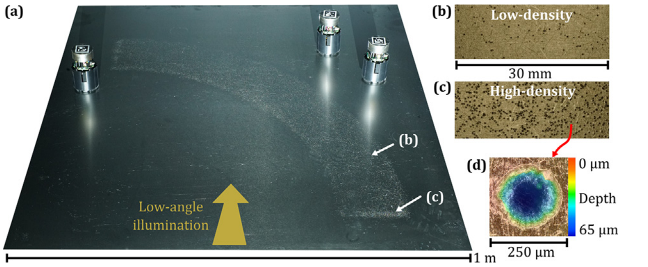

Fig. 7. (a) Patterned surface with 3 robots and detailed views of (b) low- and (c) high-density regions; and (d) depth map of a representative dimple.

Robots operate collaboratively under ergodic control, driven primarily by feature density rather than precise positioning, enabling relatively imprecise agents to create complex patterns with density gradients. Tribological testing confirms functionality of the applied dimples and their strong density dependence. An example application illustrates the complete workflow from pattern design to robot execution for a friction reducing pattern. Future work will focus on eliminating communication constraints by developing self-localization methods, making larger swarms and workpieces possible.

Declaration of competing interest

The authors declare that they have no known competing financial interests or personal relationships that could have appeared to influence the work reported in this paper.

CRediT authorship contribution statement

Malachi Landis: Writing – original draft, Visualization, Software, Methodology, Investigation, Formal analysis, Data curation. **Muye Jia:** Writing – original draft. **Annalisa T. Taylor:** Software, Methodology. **Todd D. Murphey:** Conceptualization, Funding acquisition. **Ping Guo:** Writing – review & editing, Supervision, Resources, Project administration, Funding acquisition, Conceptualization.

Acknowledgments

This work was supported by the National Science Foundation under grant number CNS-2229170. Malachi Landis is supported by the National Defence Science and Engineering Graduate (NDSEG) Fellowship.

Please cite this article as: M. Landis et al., Large-scale functional patterning using mobile robot swarms and ergodic control, CIRP Annals - Manufacturing Technology (2025), https://doi.org/10.1016/j.cirp.2025.04.044

References

[1] Kreder MJ, Alvarenga J, Kim P, Aizenberg J (2016) Design of anti-icing surfaces: smooth, textured or slippery? *Nature Reviews Materials* 1(1):1–15.
[2] Berntsson KM, Andreasson H, Jonsson PR, Larsson L, Ring K, Petronis S, Gatenholm P (2000) Reduction of barnacle recruitment on micro-textured surfaces: analysis of effective topographic characteristics and evaluation of skin friction. *Biofouling* 16(2–4):245–261.
[3] Gropper D, Wang L, Harvey TJ (2016) Hydrodynamic lubrication of textured surfaces: a review of modeling techniques and key findings. *Tribology International* 94: 509–529.
[4] Kim DE, Cha KH, Sung IH, Bryan J (2002) Design of surface micro-structures for friction control in micro-systems applications. *CIRP Annals* 51(1):495–498.
[5] Guo P, Lu Y, Ehmann KF, Cao J (2014) Generation of hierarchical micro-structures for anisotropic wetting by elliptical vibration cutting. *CIRP Annals* 63(1):553–556.
[6] García-Mayoral R, Jiménez J (2011) Drag reduction by riblets. *Philosophical transactions of the royal society A: Mathematical, physical and engineering Sciences* 369 (1940):1412–1427.
[7] Holmberg K, Erdemir A (2017) Influence of tribology on global energy consumption, costs and emissions. *Friction*, 5:263–284.
[8] Kovalchenko A, Ajayi O, Erdemir A, Fenske G, Etsion I (2004) The effect of laser texturing of steel surfaces and speed-load parameters on the transition of lubrication regime from boundary to hydrodynamic. *Tribology Transactions* 47 (2):299–307.
[9] Ramesh A, Akram W, Mishra SP, Cannon AH, Polycarpou AA, King WP (2013) Friction characteristics of microtextured surfaces under mixed and hydrodynamic lubrication. *Tribology International* 57:170–176.
[10] Schneider J, Braun D, Greiner C (2017) Laser textured surfaces for mixed lubrication: influence of aspect ratio, textured area and dimple arrangement. *Lubricants* 5(3):32.
[11] Bidkar RA, Leblanc L, Kulkarni AJ, Bahadur V, Ceccio SL, Perlin M (2014) Skin-friction drag reduction in the turbulent regime using random-textured hydrophobic surfaces. *Physics of Fluids* 26(8):085108.
[12] Park D, Han JB, Yeu T, Cho SG, Kim S, Kim H, Lee Y (2023) Development of an autonomous cleaning robot with a hydraulic manipulator arm for the cleaning of niche areas of a ship hull. *Journal of Marine Science and Engineering* 11(5):973.
[13] Song C, Cui W (2020) Review of underwater ship hull cleaning technologies. *Journal of Marine Science and Application* 19(3):415–429.
[14] Poudel L, Marques LG, Williams RA, Hyden Z, Guerra P, Fowler OL, Sha Z, Zhou W (2022) Toward swarm manufacturing: architecting a cooperative 3D printing system. *Journal of Manufacturing Science and Engineering* 144(8):081004.
[15] Gregg CE, Catanoso D, Formoso OIB, Kostitsyna I, Ochalek ME, Olatunde TJ, Park IW, Sebastianelli FM, Taylor EM, Trinh GT, Cheung KC (2024) Ultralight, strong, and self-reprogrammable mechanical metamaterials. *Science Robotics* 9(86): eadi2746.
[16] Taylor AT, Landis M, Wang Y, Murphey TD, Guo P (2024) Image to patterning: density-specified patterning of micro-structured surfaces with a mobile robot. *2024 IEEE/RSJ International Conference on Intelligent Robots and Systems (IROS)*, 2264–2270.
[17] Sorgato M, Bornillo K, Lucchetta G (2024) Reducing rubber-plastic friction in syringes through microstructured surface design and manufacturing. *CIRP Annals* .
[18] Photo of Arc de Triomphe by Jorge Láscar from Melbourne, Australia, CC BY 2.0, via Wikimedia Commons, https://commons.wikimedia.org/wiki/File:Front_view_of_the_Arc_de_Triomphe,_Paris_December_2014.jpg, Accessed April 14, 2025.
[19] Rubenstein M, Ahler C, Hoff N, Cabrera A, Nagpal R (2014) Kilobot: a low cost robot with scalable operations designed for collective behaviors. *Robotics and Autonomous Systems* 62(7):966–975.
[20] GitHub repository, https://github.com/aiml-nu/ergodic-texturing-CIRP-2025, Accessed April 14, 2025.
[21] GitHub repository, https://github.com/hbldh/bleak, Accessed April 14, 2025.
[22] Olson E (2011) AprilTag: a robust and flexible visual fiducial system. *2011 IEEE International Conference on Robotics and Automation*, 3400–3407.
[23] Tan CS, Mohd-Mokhtar R, Arshad MR (2021) A comprehensive review of coverage path planning in robotics using classical and heuristic algorithms. *IEEE Access* 9:119310–119342.
[24] Mathew G, Mezić I (2011) Metrics for ergodicity and design of ergodic dynamics for multi-agent systems. *Physica D: Nonlinear Phenomena* 240(4–5): 432–442.
[25] Miller LM, Murphey TD (2013) Trajectory optimization for continuous ergodic exploration. *2013 American Control Conference*, IEEE, , 4196–4201.
[26] Mavrommati A, Tzorakoleftherakis E, Abraham I, Murphey TD (2017) Real-time area coverage and target localization using receding-horizon ergodic exploration. *IEEE Transactions on Robotics* 34(1):62–80.
[27] Ehrenfest P, Ehrenfest T (1990) *The conceptual foundations of the statistical approach in mechanics*, Dover Publications; Mineola, New York.

Please cite this article as: M. Landis et al., Large-scale functional patterning using mobile robot swarms and ergodic control, CIRP Annals - Manufacturing Technology (2025), https://doi.org/10.1016/j.cirp.2025.04.044